Cardiovascular Science

SCIEPublish

Review

Vena Cava Occlusion Reveals Site-Specific Preload Dynamics: Implications for Volume Management in Heart Failure

Filip Konecny *

Division of Plastic Surgery, Department of Surgery, McMaster University, 101–206 James Street South, Hamilton, ON L8P 3A9, Canada

* Corresponding author. E-mail: konecny@mcmaster.ca (F.K.)

Received: 17 September 2025; Revised: 10 November 2025; Accepted: 15 February 2026; Available online: 4 March 2026

ABSTRACT: Heart failure (HF) is marked by impaired ventricular function, neurohormonal activation, and volume overload. While therapies target remodeling and neurohormonal pathways, preload management remains pivotal for symptom relief and preventing decompensation. Pressure–volume (PV) loop analysis enables precise characterization of cardiac performance during acute loading changes. To define the differential hemodynamic impact of transient inferior vena cava occlusion (IVCO) versus superior vena cava occlusion (SVCO) using PV loop analysis in a large-animal model. Controlled IVCO and SVCO were performed in healthy animals to reduce preload. PV-derived indices included stroke volume (SV), cardiac output (CO), end-systolic elastance (Ees), volume-axis intercept (V_0), and preload recruitable stroke work (PRSW). IVCO, removing ~70% of venous return, produced a marked leftward PV loop shift, decreased SV and CO, and a near-zero V_0, consistent with near-complete ventricular unloading. The end-systolic pressure–volume relationship steepened, suggesting an acute compensatory inotropic response, though Ees remained unchanged, indicating preserved intrinsic contractility. In contrast, SVCO (~30% venous return) caused only modest PV loop shifts, with preserved end-diastolic volume and stable or slightly rightward V_0. Across both interventions, preload, not intrinsic contractility, accounted for changes in mechanical work and PRSW. IVCO and SVCO elicit distinct preload-dependent hemodynamic profiles. Interpretation of PV loop–derived metrics must account for dynamic loading conditions. These findings provide mechanistic insight into acute volume regulation and warrant validation in HF-specific models to inform decongestive management strategies.

Keywords: Transient preload reduction; IVC *vs*. SVC occlusion; HF with preserved ejection fraction (HFpEF)

1. Volume Management and Preload Modulation in Heart Failure: Mechanisms, Therapeutic Implications, and Experimental Methodologies

Heart failure (HF) remains a major global health challenge, with congestion being the leading cause of hospitalization [1]. While guideline-directed medical therapy (GDMT) targets maladaptive remodeling, effective volume management is essential to prevent decompensation. Strategies include diuretics, sodium restriction, and monitoring of weight, symptoms, and biomarkers such as natriuretic peptides, troponin,

galectin-3, and ST2. Current practice prioritizes non-invasive imaging and biomarker assessment, reserving invasive hemodynamic monitoring for advanced or acute cases [2,3]. Preload manipulation provides a dynamic assessment of ventricular function by transiently increasing end-diastolic pressure (EDP) and volume (EDV), engaging the Frank-Starling mechanism. This approach can uncover latent abnormalities in contractility, compliance, and ventricular-arterial coupling (Ea/Ees), which are often impaired in HF with preserved ejection fraction (HFpEF) due to arterial stiffness and diastolic dysfunction. Elevated EDP and end-systolic pressure (ESP) in HFpEF reflect reduced compliance and increased afterload, contributing to increased myocardial workload and an increased risk of arrhythmias. Recent work emphasizes the diagnostic value of invasive hemodynamic assessment during exercise and preload modulation for accurate HFpEF phenotyping [4] and highlights the potential of non-invasive modalities such as diastolic stress echocardiography and strain imaging for dynamic evaluation [5]. Hemodynamic monitoring has evolved from invasive catheter-based techniques (e.g., pulmonary artery catheter, PiCCO) to less invasive options, including implantable sensors such as CardioMEMS and advanced imaging modalities [6]. While invasive methods provide precise measurements, they carry procedural risks and require expertise. Non-invasive techniques such as echocardiography and MRI offer safer alternatives but may lack accuracy under dynamic conditions. Combining invasive and non-invasive approaches can optimize assessment and management, ensuring accurate diagnosis and monitoring [7]. This combination ensures a more complete understanding of the patient's hemodynamic status [8]. Furthermore, innovative experimental models using tunable soft robotic sleeves have demonstrated controlled preload and afterload modulation in HFpEF physiology, enabling precise evaluation of device performance and ventricular mechanics [9]. Despite these advances, there is limited evidence on how transient preload manipulation can be leveraged to reveal subclinical abnormalities in ventricular mechanics and ventricular-arterial coupling, particularly in HFpEF. Most current assessments rely on static measurements, which may fail to capture dynamic changes in hemodynamics. This study aims to evaluate the impact of controlled preload alteration on pressure-volume relationships and coupling indices. This article seeks to determine whether dynamic hemodynamic testing can improve phenotyping and risk stratification in HF care.

2. Preload and Afterload Manipulation in Preclinical Heart Failure Models: Hemodynamic, Pressure-Volume Loop, and Autonomic Responses to Vena Cava Occlusion

Comparing methodologies for preload and afterload manipulation in preclinical heart failure (HF) animal models is essential for understanding how different experimental setups and measurement techniques influence cardiac outcomes. Preload, governed by the Frank-Starling mechanism, defines the relationship between stroke volume (SV) and end-diastolic volume (EDV), reflecting the heart's ability to augment SV in response to increased ventricular filling, provided other factors remain constant. This relationship is modulated by venous return, blood volume, and ventricular compliance, making precise and reproducible techniques critical for assessing cardiac function in HF models. Experimental techniques for manipulating afterload in animal models include pharmacologic agents such as phenylephrine to increase afterload and nitroprusside to decrease it, as well as mechanical methods like aortic balloon occlusion and external aortic compression (Tables 1–3). Vasoactive infusions can also modulate systemic vascular resistance, thereby altering afterload. These interventions influence pressure-volume (PV) loops by shifting the end-systolic pressure-volume relationship (ESPVR) rightward with increased afterload, reflecting greater pressure generation at higher end-systolic volumes without intrinsic changes in contractility.

Preload manipulation can be achieved via fluid infusion, leg elevation, pharmacologic agents (e.g., vasopressors), or experimentally through transient vena cava occlusion (VCO), a widely accepted and controllable technique. The inferior vena cava (IVC) contributes approximately 70% of total venous return from the lower body (legs, pelvis, abdomen). When the IVC is occluded, left ventricular (LV) preload drops substantially as less blood fills the ventricle. On a pressure-volume (PV) loop, this results in a leftward shift

with a corresponding reduction in SV and cardiac output via the Otto-Frank-Starling mechanism. The V_0 intercept (volume-axis intercept of ESPVR) approaches zero, indicating near-complete LV unloading as the ventricle contracts toward its minimal volume (Figure 1). In early stages of preload reduction, ESPVR may transiently steepen due to compensatory inotropy, though myocardial contractility itself typically remains constant unless stimulated by neurohumoral activation, please see succinct summary in Table 4.

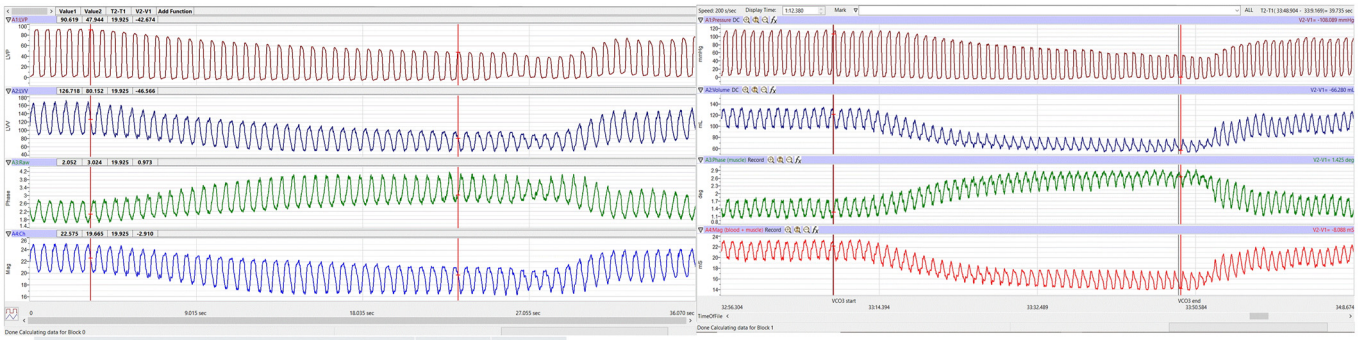

SWINE assessment of IVCO quality (N=7)	Mean	SEM
LV Volume decline (ml/sec)	3.66	0.28
LV volume drop before and at the end of IVC (ml)	44.56	4.94
LV speed of P decline (mmHg/sec)	2.65	0.22
IVC LV P drop in (sec) max-to min	14.40	0.48

SWINE assessment of SVCO quality (N=8)	Mean	SEM		T test (p value)
LV Volume decline (ml/sec)	1.39	0.08		0.00014
LV volume drop before and at the end of SVC (ml)	39.90	2.57		0.39263
LV speed of P decline (mmHg/sec)	1.19	0.14		0.00005
IVC LV P drop in (sec) max-to min	28.75	1.87		0.00005

Figure 1. Comparative Hemodynamic Effects of IVC *vs*. SVC Occlusion on Left Ventricular Pressure-Volume Dynamics. During the preload reduction phase, the left ventricular (LV) pressure should decline at a rate proportional to the decrease in LV volume. This figure with tables (N = 7 and 8 resp.,) summarizes the rate of LV volume decline (mL/s), the total volume reduction (mL), the time delay between volume decline and pressure response (s), and the rate (slope) of LV pressure decline (mmHg/s). Differences in values are reported as a *p* value. When comparing the two methods, LV volume declines more rapidly during IVC occlusion (IVCO) because occluding the IVC transiently limits a greater portion of preload volume (approximately 70/30 over time). However, the total amount of preload volume removed is ultimately similar between IVCO and SVCO. For LV pressure (LVP), both the rate of pressure decline and the speed of LV volume reduction are significantly faster with IVCO. The final volume reduction achieved is comparable between the two conditions, but the time required to reach it differs, with IVCO reaching the endpoint more quickly.

Table 1. IVCO characteristics in swine preclinical model # Shortly (<10 s) inflating a balloon catheter in the IVC, same balloon catheter position and filling volume, with 3–6 repeats. A new intervention was performed only when the baseline values from the period before the previous intervention had been restored; all recordings were done during prolonged apnea at end expiration. ## rapid transient aortic occlusion (AO) was performed to increase LV ESP by 30 to 40 mmHg within mechanical diastole, such that on the proceeding ejection, occurred from a constant EDV but against an elevated aortic pressure. Rapid pulmonary arterial occlusion (PAO) was also performed to increase RV ESP 10 to 15 mmHg within mechanical diastole, such that on the proceeding ejection occurred from a constant EDV but against an elevated pulmonary arterial pressure. The hemodynamic response followed release from each partial vessel occlusion, and the animals were allowed to recover for 1 min prior to any subsequent challenges. ##* 20% contrast in normal saline was delivered into the balloon at 0.5 ATM of pressure until occlusion of the SVC was achieved### reduce preload and record 10–12 consecutive beats as described above. Make sure systolic blood pressure remains >60 mmHg and no arrhythmias interfere with the measurements.

Animal	Animal Weight (Kg)/Age	Preload/Afterload Balloon Catheter	Preload/Afterload (AL) Occluder	Publication Refs./PMID	Inflation Device	Specified Methodology, Solution When Inflating
Swine	53–57 kg	36-to 40-mm size balloon (AGA Medical, Minneapolis)	Not used	Jani et al. [10]	BasixCOMPAK™Inflation Device	mix of iodine contrast with saline
Swine	68 kg	Valvuloplasty, 20 mm, balloon (Osypka)/Aortic balloon occlusion	Also: Intra-aortic AL occlusion	Berboth et al. [11]	not specified	not specified
Swine	47.8 ± 3.3 kg German landrace	8F balloon catheter (62080822F, Edwards Lifesciences) placed in the IVC	Also: Intra-aortic AL occlusion	Habigt et al. [12]	not specified	#
Swine	27 kg	Fogarty balloon occlusion catheter, 7F, (Edwards Lifesciences)	Not used	Mohyuddin et al. [13]	not specified	not specified
Swine	35 kg yorkshire, 45 kg Gottingen	Fogarty balloon occlusion catheter, 8F, 28 mm	Not used	McCall et al. [14]	BasixCOMPAK™Inflation Device	mix of iodine contrast with saline
Swine	81 ± 6 kg (5.5 ± 0.8 months old)	25 mm Fogarty balloon (Edwards Transfemoral Balloon Catheter, 9350BC25)	Not used	Monge García et al. [15]	not specified	#*
piglet	17 ± 5 kg or 5-to 7-week-old	not used	umbilical tape snare L and R outflow	Pinsky et al. [16]	not used	##
Swine	34 ± 2 kg	Valvuloplasty Z-Med Tyshak II, 20 mm, on 12F	Not used	Weil et al. [17]	BasixCOMPAK™Inflation Device	with isotonic saline solution.
Swine	Adult swine	CODA balloon, 32-cc endovascular balloon (Cook Medical)	Not used	Kapur et al. [18]	preCARDIA device,	##*
Swine	60–70 kg	8F Fogarty catheter	Not used	Ellenbroek et al. [19]	not specified	###
Swine	21 to 33 kg Pietran	6F Fogarty balloon catheter (Baxter Healthcare)	Not used	Morimont et al. [20]	not specified	not specified
Swine	31.0–37.2 kg	36-to 40-mm size balloon (AGA Medical, Minneapolis, Minn)	Not used	Kutty et al. [21]	not specified	isotonic saline solution

Swine	50–60 kg Landrace	not used	umbilical tape on the vena cava	Mikhova et al. [22]	not used	a transient cessation in ventilation during the steady state
Swine	35 ± 2 kg	8F Fogarty large balloon occlusion catheter in the IVC through the right femoral vein	Not used	Lionetti et al. [23]	not further specified	decrease of the Pmax by 20%
Swine	27–30 kg	14F Balloon occlusion cath. thru fem.v, at the level of the apex of the heart	Not used	Marshall et al. [24]	not further specified	not specified
Swine	16–28 kg	6F Fogarty balloon catheter (Baxter Healthcare (IVC thru fem.v)	Not used	Morimont et al. [25]	not further specified	not specified
Swine	30–40 kg Yucatan (14 m old)	14F balloon occlusion catheter	Not used	McDonald et al. [26]	not further specified	transient occlusion (catheter at the level of the apex)
Swine	31 ± 5 kg	36-mm size balloon (AGA Medical, Plymouth, Minnesota)	Not used	Schmitt et al. [27]	not further specified	inflated with isotonic saline solution
Swine	32 kg	8F Foley balloon catheter inflated to 5 mL	Not used	Miranda et al. [28]	Unknown (during CT)	water
Swine	20–30 kg	6F Fogarty balloon catheter	Not used	Lambermont et al. [29]	not specified	not specified
Swine	31–44 kg	7F Fogarty (IVC through RA)/and Aortic Balloon Occlusion (descending Ao)	also: Intra-aortic AL occlusion	Haney et al. [30]	not specified	not specified
Swine	not specified	Not balloon IVC	tape snare on IVC	Lewis et al. [31]	not further specified	not specified
Swine	40.7 ± 2.4 kg	8-F Fogarty venous thrombectomy catheter	Not used	Tayama et al. [32]	not further specified	not specified
Minipig	6 weeks of age	5F Fogarty (IVC through fem.v) atrial septostomy catheter (Baxter Health)	Not used	Cassidy et al. [33]	not further specified	air (5–10 s) inflation, no HR change during IVCO

Table 2. Characteristics of Inferior Vena Cava (IVC) Occlusion in a Sheep Preclinical Model. Comprehensive overview of inferior vena cava (IVC) occlusion characteristics in the sheep preclinical model. This table outlines the technique, occlusion site selection, catheter placement considerations, and the expected hemodynamic sequelae, including preload reduction dynamics, reflex activation, and cycle-to-cycle pressure–volume alterations. Species-specific anatomical constraints and variability are also described to contextualize model selection and facilitate comparison with other large-animal systems.

Animal	Animal Weight (Kg)/Age	Preload/Afterload Balloon Catheter	Preload/Afterload (AL) Occluder	Publication Refs./PMID	Inflation Device	Specified Methodology, Solution When Inflating
Sheep	48.7 ± 6.2 kg	not used	Rummel Tourniquet	Brunel et al. [34]	not used	during end expiration breath-holds with temporary occlusion of the IVC
Sheep	adult	8F balloon catheter was positioned in the inferior vena	Not used	Giao et al. [35]	not further specified	not specified
Sheep	40.5 ± 6.8 kg	not used	snares on the IVC and distal descending thoracic aorta	Wo et al. [36]	not used	IVC and Ao snare was tightened over ~10 s in all animals to produce a transient preload/afterload maneuver for later LV pressure–volume loop analysis
Sheep	59.0 ± 7.1 kg	36F Fogarty catheter placed in the inferior vena cava	Not used	Mau et al. [37]	not further specified	not specified
Sheep	39.4 ± 1.4 kg	Vena cava via the femoral vessels	Not used	Yerebakan et al. [38]	not further specified	not specified
Sheep	26 ± 4.5 kg	not used	2 snares placed on the IVC and left PA	Grignola et al. [39]	not used	open chest and pericardium at steady-state conditions and during vena cava occlusion
Sheep	16.6 ± 3.7 kg	not used	a string	Leeuwenburgh et al. [40]	not used	relationships were obtained by means of preload reduction with a string around the inferior vena cava
Sheep	53.4 ± 4 kg	22-F Fogarty, (Baxter International)	Not used	Ramanathan et al. [41]	not further specified	not specified
Lamb	3.1–7.8 kg	balloon catheter	not used	Cardozo et al. [42]	not specified	balloon catheter was placed in the IVC via the left or right femoral vein to change preload conditions for the ventricles
Sheep	19.4 ± 4.1 kg	not used	nylon tape	Hon et al. [43]	not used	open chest placement of nylon tape by lifting the tape around the inferior vena cava for no more than 10 s. All measurements were taken at the end of expiration with the ventilator turned off
Fetal Sheep	d 133 of gestation	inflating the caval balloon with 0.75 mL of saline over period of 6 to 8 s	acaval balloon	Lewinsky et al. [44]	not further specified	Three IVC occlusions were performed at each level of embolization, with full recovery confirmed by return to pre-occlusion heart rate and LV pressures and volumes. SVC occlusion was compared with IVC occlusion in one animal.

Sheep	26.8 + 3.2 kg	aortic occluder balloon	electropneumatic aortic occluder	Gupta et al. [45]	intra-aortic occluder balloon-control system	Principle of Operation in M&M

Table 3. Techniques are used to transiently reduce preload in canine models. Various methods have been employed, including pneumatic cuffs, hydraulic vascular occlusion devices, rubber tourniquets, and sutures placed beneath the inferior vena cava (IVC). Additionally, umbilical tape has been utilized for controlled, reversible IVC constriction. These techniques allow for the acute modulation of venous return to study cardiac preload dependence and hemodynamic responses in experimental settings

Animal	**Animal Weight (Kg)/Age**	**Preload/Afterload Balloon Catheter**	**Preload/Afterload (AL) Occluder**	**Publication Refs./PMID**	**Inflation Device**	**Specified Methodology, Solution When Inflating**
Dog mongrel	20–25 kg	not used	Via partial inflation of the vena cava occluders	Ahmadian et al. [46]	not further specified	not further specified
Dog	27.2 ± 3.0 kg	not used	suture placed around the IVC	Gruslova et al. [47]	not further specified	not further specified
Dog	Beagle 13.7 ± 0.4 kg	7F TyshakII (IVC balloon diameter: 12 mm, balloon length: 3 cm)	NA	Mathieu et al. [48]	not further specified	successful inferior vena cava occlusion (IVCO) was a mean arterial pressure of 50 mm Hg or less
Dog mongrel	14–18 kg	not used	Rubber tourniquet	Iwade et al. [49]	not further specified	Reduced LV end-diastolic volume by transient IVC occlusion during a brief (<5 s) apnea at zero airway pressure until LV end systolic pressure decreased to below 15 mmHg. A minimum of 60 s separated each sequential preload-reducing maneuver.
Dog Mongrel	23 ± 5 kg	not used	A pneumatic cuff/constrictor	Sun et al. [50]	(*In Vivo* Metrics, Healdsburg, CA)	gradual occlusion of the IVC with the rubber tourniquet, approximately a 20-mmHg decline in LV systolic pressure over 8 to 12 cardiac cycles
Dog mongrel	0.5–1 y.o/old 7–10 y.o young	not used	Pneumonic inferior vena cava occluder	Munagala et al. [51]	not further specified	All the data were collected with the ventilator stopped in the end-expiratory position
Dog adult	22–42 kg	not used	Caval occluder/descending Aortic occluder	Karunanithi et al. [52]	not further specified	500-mL bolus of warmed saline was given before IVCO.
Dog Mongrel	18–24 kg	not used	Rubber tourniquet	Leather et al. [53]	not further specified	the hydraulic vascular occluder, resulting in an approximately 10-mmHg decline in mean LA pressure over 10 to 15 cardiac cycles

Dog Mongrel IVC	21.5 ± 2.4 kg	i.v.hydraulic balloon catheter (Fogarty) inserted p.c. from the right external jugular vein and positioned under fluoroscopy in the intrathoracic	hydraulic occluder around intrathoracic IVC	Denault et al. [54]	not further specified	with minimal alterations in heart rate or afterload
Dog	20–25 kg	not used	Silicone pneumatic occluder	Atkins et al. [55]	not further specified	apneic IVC occlusion of positive pressure ventilation (tidal volume of 10 mL/kg, breathing frequency of 20 breaths/min, sine wave inspiratory flow)
Dog mongrel	25–30 kg	not used	Vena caval balloon cuff occluder	Hettrick et al. [56]	not further specified	not further specified
Dog Beagle	10–13 kg	not used	Balloon Occluder (AccessTechnologies, Skokie, IL)	Regan et al. [57]	not further specified	To determine load-independent parameters of cardiac contractility, transient IVCo (5–10 s per event) was performed in conscious animals after the 15 min baseline assessment and was performed 2–3 times (~5 min between each occlusion) in each animal at each time point by rapid, transient cuff inflation.
Dog Greyhounds/dog mongrel	not specified	not used	Umbilical tape is creating a snare	McKay et al. [58]	not further specified	IVCO 10 s, using a balloon Cath filled with air
Dog mongrel	20 to 25 kg	Latex balloon occluder catheter in the IVC through the right femoral vein	Not used	Kass et al. [59]	not further specified	not further specified

Table 4. Summary of key differences between inferior and superior vena cava occlusion in preclinical models, highlighting variations in preload reduction magnitude, reflex activation timing, pressure-volume loop alterations, and arrhythmic.

Parameter	IVC Occlusion	SVC Occlusion
Venous Return Affected	~70%	~30%
Preload Reduction	Substantial	Modest
PV Loop Shift	Significant leftward	Mild leftward
Baroreflex Activation	Delayed, mild tachycardia	Variable
Arrhythmic Risk	Due to afterload mismatch post-occlusion	Due to abrupt right atrial unloading

3. Materials and Methods

Study Design and Population: This comparative experimental study evaluated the hemodynamic effects of inferior vena cava occlusion (IVCO) versus superior vena cava occlusion (SVCO) on left ventricular (LV) pressure-volume dynamics. A total of 15 subjects were included in the initial groups (IVCO group: $n = 7$; SVCO group: $n = 8$). All subjects underwent invasive pressure-volume analysis under controlled conditions. Hemodynamic Measurements: Admittance PV studies were performed using an ADV500 control unit (Transonic Scisense, London, ON, Canada). Hemodynamic PV parameters were collected using the FA404 data acquisition system, and data analysis was completed with the dedicated PV module in LabScribe3 (iWorx Systems, Dover, NH, USA). Prior to catheterization, the catheter's pressure sensor was hydrated for 30 min in a 50-mL Falcon conical centrifuge tube (Thermo Fisher Scientific, Waltham, MA, USA) containing 0.9% saline or phosphate-buffered saline at 38 °C. The pressure sensor was then balanced under the meniscus of the same 38 °C solution before PV catheterization. System setting parameters, including volume mode (W), premeasured blood resistivity, and myocardial properties obtained using the manufacturer's probe, were entered into the ADV500 system. Independently assessed stroke volume from Transthoracic Echocardiography (TTE) using LV outflow Simpson's calculation was also added to the system settings. After successful system setup, catheter hydration, and 7F pressure balancing, a single-pressure sensor, 48-inch-long pigtail catheter with a variable segment length (VSL) configuration was inserted through a 9F sheath. The VSL design allowed selection of the recording segment based on ventricular size; in this study, segment spacing from 1 to 4 (30–60 mm) was used. Under fluoroscopic guidance, the catheter was advanced through either the right carotid artery or the right femoral artery into the aortic arch. When the catheter approached the LV, the pressure tracing showed a characteristic aortic waveform before crossing the aortic valve. At this point, a 0.035-inch, 150-cm J-tip guidewire was inserted through the lumen to facilitate smooth catheter advancement across the valve and enable later fine-tuning of LV positioning. Preload Reduction Protocol: Preload reduction was achieved by transient balloon inflation in either the IVC or SVC for a standardized duration sufficient to induce measurable changes in LV filling. A 14F, 100-cm usable length valvuloplasty balloon catheter with a 30-mm inflated diameter and 50-mm balloon length was used to achieve stable IVCO. The balloon length was selected to ensure a reliable seal across the intrahepatic IVC segment, while the burst pressure rating (2 ATM) and introducer compatibility facilitated safe venous access. For smaller swine (<60 kg), a 28-mm balloon diameter is suitable to ensure full occlusion without excessive wall stress. During occlusion, LV pressure and volume were sampled at high temporal resolution (≥500 Hz) to capture dynamic changes. Parameters Assessed: The following indices were derived for each occlusion maneuver: Rate of LV volume decline (mL/s), Total LV volume reduction (mL), Time delay between volume decline and pressure response (s), Rate (slope) of LV pressure decline (mmHg/s). Data Analysis: Values were summarized as mean ± SD for each group. Differences between IVCO and SVCO were assessed using unpaired *t*-tests, with statistical significance set at $p < 0.05$. Comparative trends were visualized using pressure-volume loop overlays and tabulated summaries.

In contrast, superior vena cava occlusion (SVCO) affects about 30% of venous return from the upper body. The LV does not fully unload, and EDV remains relatively preserved. On the PV loop, this manifests as a smaller leftward shift, with V_0 shifting rightward or remaining stable, reflecting incomplete ventricular unloading. The ventricle may show reduced ability to empty, potentially due to afterload mismatch or altered filling dynamics.

Swine models are particularly valuable in this context, given that their cardiovascular anatomy and physiology closely resemble those of humans [60,61]. In these models, transient IVC occlusion acutely reduces LV preload, decreasing systolic and diastolic pressures, lowering EDV, and reducing cardiac output [62]. This technique is especially valuable for studying HF pathophysiology and evaluating therapies in volume-overloaded or diuretic-resistant patients [18]. Transient VCO maneuvers reduce venous return and mean arterial pressure (MAP), triggering baroreflex-mediated compensatory responses like increased heart rate and systemic vascular resistance (SVR). Baroreflex sensitivity (BRS) can be assessed via ECG using slope and sequence methods that relate blood pressure fluctuations to heart rate variability. Experimental models have limitations, including anesthesia-induced alterations in autonomic tone, interspecies differences in reflex responses, mechanical constraints of occlusion techniques, and the confounding effects of heart rate variability on contractility indices like Ees. Acknowledging these factors is essential for ensuring critical rigor in data interpretation.

During brief transient occlusions (as typically employed in experimental settings), compensatory autonomic mechanisms like baroreflex activation, sympathetic stimulation, and RAAS engagement often remain incomplete or delayed [63]. This preserves intrinsic myocardial contractility, as indicated by stable Ees (end-systolic elastance), despite significant preload reductions. Ees calculations isolate the ventricle's contractile state, minimizing preload and afterload influences. Even though IVC occlusion markedly reduces preload (and consequently SV and CO), myocardial force-generating capacity remains stable in the absence of physiologic stimuli like β-adrenergic activation. Notably, differential volume intercepts (V_0) reflect varying degrees of ventricular unloading rather than changes in contractility, confirming Ees stability across conditions (Figure 2).

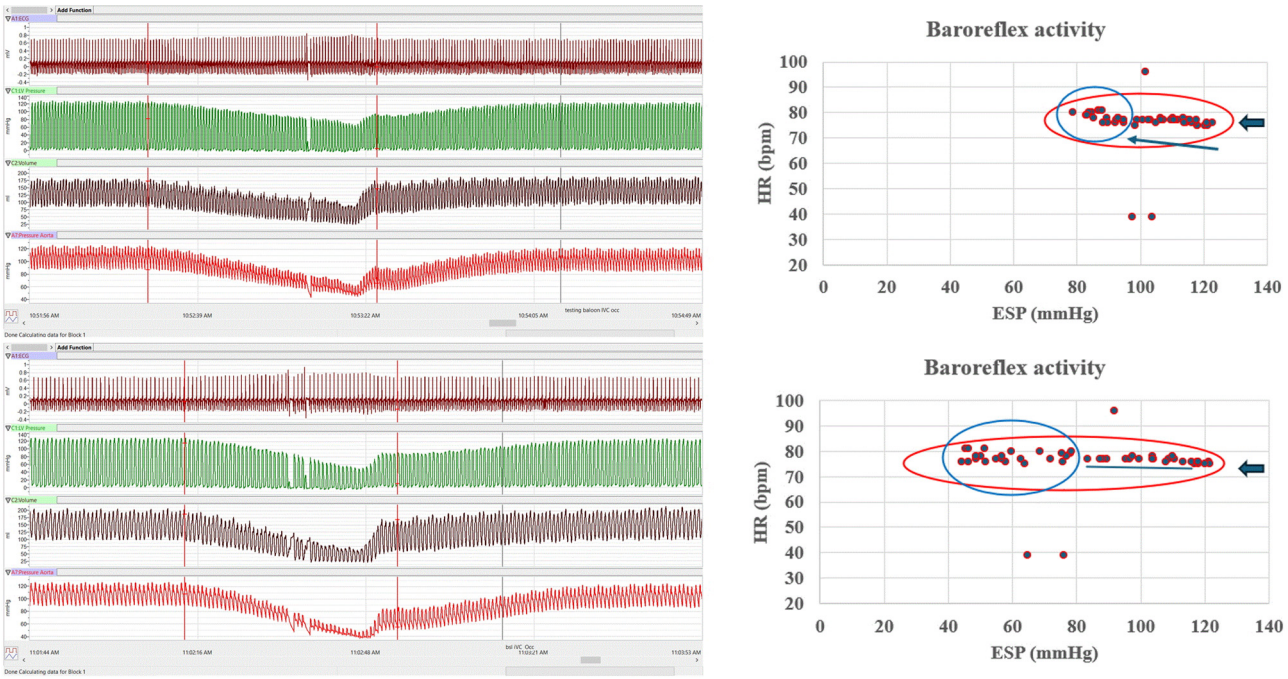

Figure 2. Baroreflex Activity During Transient Preload Reduction Using IVC Occlusion. A balloon catheter was positioned in the inferior vena cava to induce transient preload reduction. The first channel displays ECG lead II, followed by left ventricular pressure (LVP) and left ventricular volume (LVV), with aortic pressure shown in the final channel. Two sequential IVC

occlusions were performed. During the first occlusion, both pressure (P) and volume (V) decreased proportionally, demonstrating a strong PV relationship. The decline occurred at a relatively stable heart rate (HR). In the upper-right panel, the relationship between end-systolic pressure (ESP) and HR is shown, with data points tightly clustered from the onset of occlusion (blue arrow) through its completion. Near the end of the maneuver, a slight increase in HR (blue circle) is evident, consistent with activation of the neurohumoral axis, likely mediated by the arterial baroreflex. Notably, three arrhythmic beats occurred prior to the observed HR response. In the second (lower) occlusion, left ventricular pressure again decreased in parallel with volume; however, the occlusion was sustained for a longer duration. This prolonged preload reduction resulted in greater dispersion of HR values and a diminished, less distinct late HR acceleration compared with the first occlusion.

Interestingly, arterial elastance (Ea), a measure of afterload representing the net arterial load the heart ejects against, remains relatively unchanged during both IVC and SVC occlusion (Figure 3). Neither intervention directly alters arterial properties such as systemic vascular resistance or arterial compliance. Since both maneuvers primarily affect venous return (preload) without acutely changing afterload determinants, Ea stays stable. As preload drops, SV and end-systolic pressure (ESP) fall proportionally. Because Ea is calculated as ESP divided by SV, and both decrease in parallel, the ratio and thus Ea remain constant (Figure 3). Furthermore, systemic resistance typically does not change during brief preload reductions unless compensatory reflexes are triggered, which is often not the case during short experimental occlusions. Additional load-independent or minimally load-dependent indices (e.g., PRSW, dP/dt max adjusted for preload, myocardial strain) that could provide complementary insights during transient preload/afterload alterations.

Dynamic PV loop analysis reveals distinct mechanical and autonomic patterns during transient versus sustained preload alterations. In the initial IVC occlusion, parallel declines in LVP and LVV at a steady heart rate reflect a purely mechanical preload reduction. ESP and heart rate data cluster tightly, indicating preserved myocardial contractility and hemodynamic stability. A slight heart rate increase near the end of occlusion signals early baroreflex-mediated sympathetic activation in response to falling arterial pressure and reduced ventricular filling. Notably, transient arrhythmic cycles often precede autonomic compensation, indicating that sudden preload reduction can transiently destabilize conduction, especially in compromised hearts.

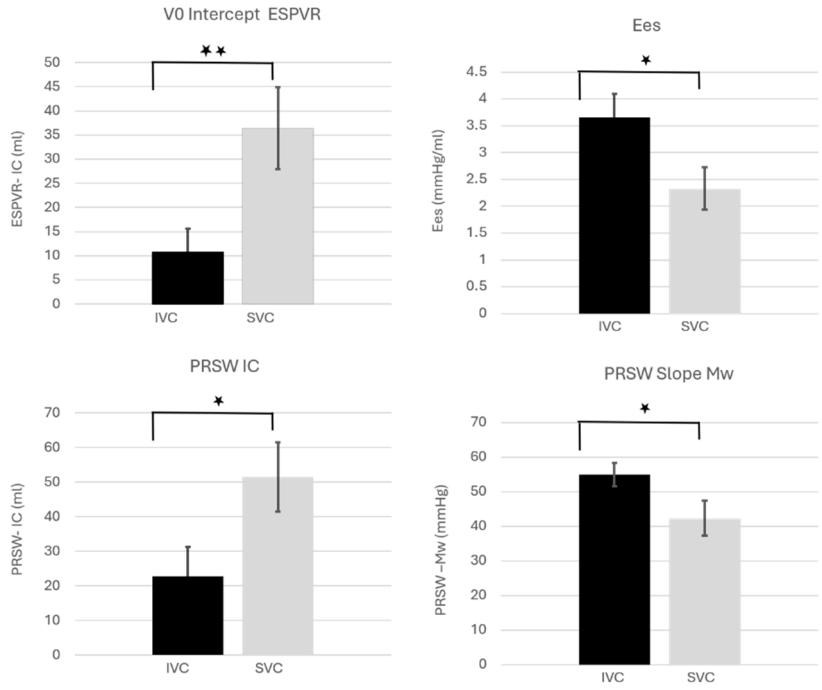

Figure 3. Later comparison of inotropic indices of cardiac contractile function in healthy swine between IVCO and SVCO. Significant differences were observed following both transient occlusion maneuvers. (N = 7 and 8, respectively; * $p < 0.05$, ** $p < 0.01$; data shown as mean ± SEM). During IVC occlusion, which disrupts approximately 70% of venous return from the

lower body, the V_0 intercept approaches zero ml, indicating substantial unloading of the left ventricular (LV) chamber. In contrast, transient SVC occlusion results in diminished LV emptying capacity, reflected by a rightward shift of the V_0 notch and signifying less effective transient unloading. Importantly, end-systolic elastance (Ees) varied significantly between the two occlusion conditions, providing novel insights into the dynamic cardio-elastic properties of the LV under acute preload reduction.

In prolonged occlusions, preload reduction continues, but with more dispersed heart rate patterns and a blunted tachycardic response. This suggests baroreflex adaptation or vagal predominance, which diminishes sympathetic compensation over time. Clinically, this pattern indicates that prolonged preload reduction may limit reflex-mediated HR adjustments, contributing to hemodynamic instability or arrhythmic risk in advanced HF. The combination of preload dependency, reduced autonomic reserve, and diastolic dysfunction in HFpEF makes this patient population particularly vulnerable [18].

If modeled further, serial evaluation of Ees and Ea during transient and sustained occlusions could clarify how contractility and afterload interact under varying loading conditions in health and HF states. In HFpEF, rapid ESP rise, elevated EDP, low arterial compliance, and increased impedance predispose to arrhythmias, particularly during SVCO, where abrupt right atrial and ventricular preload drops destabilize conduction. Conversely, post-IVCO arrhythmias likely stem from afterload mismatch as Ea rises and Ees remains impaired.

Collectively, these findings advocate cautious, controlled preload modulation in both experimental and clinical settings, particularly in patients with borderline hemodynamics or heightened arrhythmic risk. They highlight the translational relevance of standardized, reproducible preload manipulation protocols and underscore the importance of concurrently monitoring mechanical, electrophysiologic, and autonomic parameters during volume management in HF.

4. Conclusions

This review compares transient inferior vena cava occlusion (IVCO) and superior vena cava occlusion (SVCO) in a preclinical swine model to delineate their differential effects on left ventricular (LV) hemodynamics assessed by pressure-volume (PV) loop analysis. Transient IVCO, which reduces systemic venous return by approximately 70%, induces a marked preload reduction that shifts the PV loop leftward and decreases stroke volume (SV) and cardiac output (CO), while transiently steepening the ESPVR due to early, load-dependent inotropic compensation. In contrast, SVCO affects only ~30% of venous return, producing modest preload reduction and incomplete LV unloading (Figure 3). Despite these differences in loading, contractility (Ees) remained stable across both perturbations, supporting the premise that brief occlusions do not fully recruit neurohumoral compensatory systems (Table 4). Corresponding changes in PRSW, stroke work, and mechanical efficiency largely reflected altered loading conditions rather than intrinsic myocardial contractile adaptation. These results emphasize the need for careful interpretation of PV-derived contractility metrics in settings where preload and afterload fluctuate, particularly in conditions such as HFpEF, shock states, or during therapeutic interventions (e.g., diuresis, vasodilation, or mechanical support). Misinterpreting load-dependent responses as changes in intrinsic myocardial function could lead to incorrect conclusions about contractile reserve, disease progression, or treatment efficacy. Importantly, the differential venous territories affected by SVCO and IVCO, upper systemic/cerebral *vs*. splanchnic and lower systemic, may variably influence right-sided filling dynamics and pulmonary pressures, which could secondarily modify LV preload. Although not directly assessed here, this highlights a key physiological interaction and a potential area for more detailed biventricular assessment in future experiments.

While the current analysis primarily focused on systolic metrics, diastolic behavior represents another important avenue for investigation. Load-dependent shifts in the end-diastolic pressure-volume relationship (EDPVR), filling pressures, or relaxation parameters could provide deeper insight into changes in ventricular compliance during transient preload alterations. Such information may be particularly relevant

for translational modeling of HFpEF, where diastolic stiffness and impaired reserve are central pathophysiologic features. The heart rate (HR) responses observed in this study further underscore the dynamic nature of autonomic engagement during transient loading shifts. During IVCO, parallel declines in LV pressure and volume confirmed effective preload reduction, with HR initially stable but demonstrating a modest rise toward the end of the occlusion, consistent with early baroreflex activation (Figure 2). This response was most apparent during the initial brief occlusion, in which ESP–HR data remained tightly clustered until a small HR increase followed several arrhythmic beats. In contrast, the second, longer occlusion produced a more variable and attenuated HR response, suggesting a dampened baroreflex response, possibly related to limitations in vagal withdrawal, baroreceptor resetting, or reduced sympathetic recruitment. These findings support the concept that baroreflex sensitivity is time-dependent and more robust during brief perturbations (Table 4). Overall, the translational value of this work lies in demonstrating that not all preload-reducing maneuvers are physiologically equivalent. Understanding how different occlusion strategies alter cardiac loading, autonomic responses, and PV-derived contractility indices provides a more accurate framework for interpreting load-independent metrics, validating computational models, and refining experimental protocols for both healthy and HFpEF phenotypes. Future work incorporating biventricular assessment, diastolic function, longer perturbation paradigms, and integrative neurohumoral measurements would further strengthen the mechanistic insight and clinical applicability of this preclinical model.

Statement of the Use of Generative AI and AI-Assisted Technologies in the Writing Process

During the preparation of this manuscript, the authors used Microsoft Copilot to support drafting and editing. All content generated by the tool was reviewed and revised as necessary, and the authors take full responsibility for the final published work.

Ethics Statement

Ethical review and approval were waived due to the analysis of existing data. Study was based on a retrospective record review, examining historical data without active intervention, and use of de-identified datasets and specimens.

Informed Consent Statement

Not Applicable.

Data Availability Statement

The data that support the findings of this study are available from the corresponding author upon reasonable request.

Funding

This research received no external funding.

Declaration of Competing Interest

The author declares that he has no known competing financial interests or personal relationships that could have appeared to influence the work reported in this paper.

References

1. Ponikowski P, Voors AA, Anker SD, Bueno H, Cleland JGF, Coats AJS, et al. 2016 ESC Guidelines for the diagnosis and treatment of acute and chronic heart failure: The Task Force for the diagnosis and treatment of acute and chronic heart

failure of the European Society of Cardiology (ESC). Developed with the special contribution of the Heart Failure Association (HFA) of the ESC. *Eur. Heart J.* **2016**, *37*, 2129–2200. DOI:10.1093/eurheartj/ehw128; Erratum in *Eur. Heart J.* **2018**, *39*, 860. DOI:10.1093/eurheartj/ehw383

2. Heidenreich PA, Bozkurt B, Aguilar D, Allen LA, Byun JJ, Colvin MM, et al. 2022 AHA/ACC/HFSA Guideline for the Management of Heart Failure: A Report of the American College of Cardiology/American Heart Association Joint Committee on Clinical Practice Guidelines. *Circulation* **2022**, *145*, e895–e1032. DOI:10.1161/CIR.0000000000001063; Erratum in *Circulation* **2023**, *147*, e674. DOI:10.1161/CIR.0000000000001142
3. McDonagh TA, Metra M, Adamo M, Gardner RS, Baumbach A, Böhm M, et al. 2021 ESC Guidelines for the diagnosis and treatment of acute and chronic heart failure: Developed by the Task Force for the diagnosis and treatment of acute and chronic heart failure of the European Society of Cardiology (ESC). With the special contribution of the Heart Failure Association (HFA) of the ESC. *Eur. J. Heart Fail.* **2022**, *24*, 4–131. DOI:10.1002/ejhf.2333
4. Wattanachayakul P, Kittipibul V, Salah HM, Yaku H, Gustafsson F, Baratto C, et al. Invasive haemodynamic assessment in heart failure with preserved ejection fraction. *ESC Heart Fail.* **2025**, *12*, 1558–1570. DOI:10.1002/ehf2.15163
5. Rosalia L, Ozturk C, Wang SX, Quevedo-Moreno D, Saeed MY, Mauskapf A, et al. Modulating Cardiac Hemodynamics Using Tunable Soft Robotic Sleeves in a Porcine Model of HFpEF Physiology for Device Testing Applications. *Adv. Funct. Mater.* **2024**, *34*, 2310085. DOI:10.1002/adfm.202310085
6. Vyas R, Patel M, Khouri SJ, Moukarbel GV. A profile on the CardioMEMS HF system in the management of patients with early stages of heart failure: An update. *Expert Rev. Med. Devices* **2023**, *20*, 621–631. DOI:10.1080/17434440.2023.2228683
7. Sharifov OF, Gupta H. What Is the Evidence That the Tissue Doppler Index E/e' Reflects Left Ventricular Filling Pressure Changes After Exercise or Pharmacological Intervention for Evaluating Diastolic Function? A Systematic Review. *J. Am. Heart Assoc.* **2017**, *6*, e004766. DOI:10.1161/JAHA.116.004766
8. Opotowsky AR, Hess E, Maron BA, Brittain EL, Barón AE, Maddox TM, et al. Thermodilution vs Estimated Fick Cardiac Output Measurement in Clinical Practice: An Analysis of Mortality from the Veterans Affairs Clinical Assessment, Reporting, and Tracking (VA CART) Program and Vanderbilt University. *JAMA Cardiol.* **2017**, *2*, 1090–1099. DOI:10.1001/jamacardio.2017.2945
9. Istratoaie S, Frost CL, Donal E. Non-Invasive Hemodynamic Assessment of Heart Failure with Preserved Ejection Fraction. *Korean Circ. J.* **2025**, *55*, 165–184. DOI:10.4070/kcj.2024.0370
10. Jani V, Konecny F, Shelby A, Kulkarni A, Hammel J, Schuster A, et al. Influence of right ventricular pressure and volume overload on right and left ventricular diastolic function. *J. Thorac. Cardiovasc. Surg.* **2022**, *163*, e299–e308. DOI:10.1016/j.jtcvs.2021.07.040
11. Berboth L, Zirngast B, Manninger M, Steendijk P, Tschöpe C, Scherr D, et al. Graded lower body negative pressure induces intraventricular negative pressures and incremental diastolic suction: A pressure-volume study in a porcine model. *J. Appl. Physiol.* **2022**, *133*, 20–26. DOI:10.1152/japplphysiol.00110.2022
12. Habigt MA, Krieger M, Gesenhues J, Ketelhut M, Mechelinck M, Hein M. Non-linearity of end-systolic pressure-volume relation in afterload increases is caused by an overlay of shortening deactivation and the Frank-Starling mechanism. *Sci. Rep.* **2021**, *11*, 3353. DOI:10.1038/s41598-021-82791-3
13. Mohyuddin R, Dietrichs ES, Sundaram P, Kondratiev T, Figenschou MF, Sieck GC, et al. Cardiovascular Effects of Epinephrine During Experimental Hypothermia (32 °C) With Spontaneous Circulation in an Intact Porcine Model. *Front. Physiol.* **2021**, *12*, 718667. DOI:10.3389/fphys.2021.718667
14. McCall FC, Telukuntla KS, Karantalis V, Suncion VY, Heldman AW, Mushtaq M, et al. Myocardial infarction and intramyocardial injection models in swine. *Nat. Protoc.* **2012**, *7*, 1479–1496. DOI:10.1038/nprot.2012.075
15. Monge García MI, Jian Z, Hatib F, Settels JJ, Cecconi M, Pinsky MR. Dynamic Arterial Elastance as a Ventriculo-Arterial Coupling Index: An Experimental Animal Study. *Front. Physiol.* **2020**, *11*, 284. DOI:10.3389/fphys.2020.00284
16. Pinsky MR. Dynamic right and left ventricular interactions in the pig. *Exp. Physiol.* **2020**, *105*, 1293–1315. DOI:10.1113/EP088550
17. Weil BR, Techiryan G, Suzuki G, Konecny F, Canty JM, Jr. Adaptive Reductions in Left Ventricular Diastolic Compliance Protect the Heart From Stretch-Induced Stunning. *JACC Basic Transl. Sci.* **2019**, *4*, 527–541. DOI:10.1016/j.jacbts.2019.04.002
18. Kapur NK, Kiernan MS, Gorgoshvili I, Yousefzai R, Vorovich EE, Tedford RJ, et al. Intermittent Occlusion of the Superior Vena Cava to Improve Hemodynamics in Patients With Acutely Decompensated Heart Failure: The VENUS-HF Early Feasibility Study. *Circ. Heart Fail.* **2022**, *15*, e008934. DOI:10.1161/CIRCHEARTFAILURE.121.008934
19. Ellenbroek GH, van Hout GP, Timmers L, Doevendans PA, Pasterkamp G, Hoefer IE. Primary Outcome Assessment in a Pig Model of Acute Myocardial Infarction. *J. Vis. Exp.* **2016**, *116*, 54021. DOI:10.3791/54021

20. Morimont P, Guiot J, Desaive T, Tchana-Sato V, Janssen N, Cagnina A, et al. Veno-venous extracorporeal CO_2 removal improves pulmonary hemodynamics in a porcine ARDS model. *Acta Anaesthesiol. Scand.* **2015**, *59*, 448–456. DOI:10.1111/aas.12497
21. Kutty S, Kottam AT, Padiyath A, Bidasee KR, Li L, Gao S, et al. Validation of admittance computed left ventricular volumes against real-time three-dimensional echocardiography in the porcine heart. *Exp. Physiol.* **2013**, *98*, 1092–1101. DOI:10.1113/expphysiol.2012.070821
22. Mikhova KM, Don CW, Laflamme M, Kellum JA, Mulligan MS, Verrier ED, et al. Effect of cytokine hemoadsorption on brain death-induced ventricular dysfunction in a porcine model. *J. Thorac. Cardiovasc. Surg.* **2013**, *145*, 215–224. DOI:10.1016/j.jtcvs.2012.08.002
23. Lionetti V, Romano SL, Bianchi G, Bernini F, Dushpanova A, Mascia G, et al. Impact of acute changes of left ventricular contractility on the transvalvular impedance: validation study by pressure-volume loop analysis in healthy pigs. *PLoS ONE* **2013**, *8*, e80591. DOI:10.1371/journal.pone.0080591
24. Marshall KD, Muller BN, Krenz M, Hanft LM, McDonald KS, Dellsperger KC, et al. Heart failure with preserved ejection fraction: chronic low-intensity interval exercise training preserves myocardial O_2 balance and diastolic function. *J. Appl. Physiol.* **2013**, *114*, 131–147. DOI:10.1152/japplphysiol.01059.2012
25. Morimont P, Lambermont B, Desaive T, Janssen N, Chase G, D'Orio V. Arterial dP/dtmax accurately reflects left ventricular contractility during shock when adequate vascular filling is achieved. *BMC Cardiovasc. Disord.* **2012**, *12*, 13. DOI:10.1186/1471-2261-12-13
26. McDonald KS, Hanft LM, Domeier TL, Emter CA. Length and PKA Dependence of Force Generation and Loaded Shortening in Porcine Cardiac Myocytes. *Biochem. Res. Int.* **2012**, *2012*, 371415. DOI:10.1155/2012/371415
27. Schmitt B, Steendijk P, Lunze K, Ovroutski S, Falkenberg J, Rahmanzadeh P, et al. Integrated assessment of diastolic and systolic ventricular function using diagnostic cardiac magnetic resonance catheterization: validation in pigs and application in a clinical pilot study. *JACC Cardiovasc. Imaging* **2009**, *2*, 1271–1281. DOI:10.1016/j.jcmg.2009.09.007
28. Miranda DR, Klompe L, Cademartiri F, Haitsma JJ, Palumbo A, Takkenberg JJ, et al. The effect of open lung ventilation on right ventricular and left ventricular function in lung-lavaged pigs. *Crit. Care* **2006**, *10*, R86. DOI:10.1186/cc4944
29. Lambermont B, Ghuysen A, Kolh P, Tchana-Sato V, Segers P, Gérard P, et al. Effects of endotoxic shock on right ventricular systolic function and mechanical efficiency. *Cardiovasc. Res.* **2003**, *59*, 412–418. DOI:10.1016/s0008-6363(03)00368-7
30. Haney MF, Johansson G, Häggmark S, Biber B. Method of preload reduction during LVPVR analysis of systolic function: Airway pressure elevation and vena cava occlusion. *Anesthesiology* **2002**, *97*, 436–446. DOI:10.1097/00000542-200208000-00022
31. Lewis ME, Al-Khalidi AH, Bonser RS, Clutton-Brock T, Morton D, Paterson D, et al. Vagus nerve stimulation decreases left ventricular contractility *in vivo* in the human and pig heart. *J. Physiol.* **2001**, *534 Pt 2*, 547–552. DOI:10.1111/j.1469-7793.2001.00547.x
32. Tayama M, Solomon SB, Glantz SA. Effect of lidocaine on left ventricular pressure-volume curves during demand ischemia in pigs. *Am. J. Physiol.* **1998**, *274*, H2100–H2109. DOI:10.1152/ajpheart.1998.274.6.H2100
33. Cassidy SC, Chan DP, Allen HD. Left ventricular systolic function, arterial elastance, and ventricular-vascular coupling: A developmental study in piglets. *Pediatr. Res.* **1997**, *42*, 273–281. DOI:10.1203/00006450-199709000-00005
34. Brunel L, Williams ZA, Yata M, Robinson BM, Wise IK, Paterson HS, et al. Incorporating the anterior mitral leaflet to the annulus impairs left ventricular function in an ovine model. *JTCVS Open* **2021**, *7*, 111–120. DOI:10.1016/j.xjon.2021.03.010
35. Giao DM, Wang Y, Rojas R, Takaba K, Badathala A, Spaulding KA, et al. Left ventricular geometry during unloading and the end-systolic pressure volume relationship: Measurement with a modified real-time MRI-based method in normal sheep. *PLoS ONE* **2020**, *15*, e0234896. DOI:10.1371/journal.pone.0234896
36. Wo N, Rajagopal V, Cheung MMH, Smolich JJ, Mynard JP. Assessment of single beat end-systolic elastance methods for quantifying ventricular contractility. *Heart Vessels* **2019**, *34*, 716–723. DOI:10.1007/s00380-018-1303-5
37. Mau J, Menzie S, Huang Y, Ward M, Hunyor S. Nonsurround, nonuniform, biventricular-capable direct cardiac compression provides Frank-Starling recruitment independent of left ventricular septal damage. *J. Thorac. Cardiovasc. Surg.* **2011**, *142*, 209–215. DOI:10.1016/j.jtcvs.2010.05.057
38. Yerebakan C, Klopsch C, Prietz S, Boltze J, Vollmar B, Liebold A, et al. Pressure-volume loops: Feasible for the evaluation of right ventricular function in an experimental model of acute pulmonary regurgitation? *Interact. Cardiovasc. Thorac. Surg.* **2009**, *9*, 163–168. DOI:10.1510/icvts.2008.198275
39. Grignola JC, Ginés F, Guzzo D. Comparison of the Tei index with invasive measurements of right ventricular function. *Int. J. Cardiol.* **2006**, *113*, 25–33. DOI:10.1016/j.ijcard.2005.10.012
40. Leeuwenburgh BP, Helbing WA, Steendijk P, Schoof PH, Baan J. Effects of acute left ventricular unloading on right

ventricular function in normal and chronic right ventricular pressure-overloaded lambs. *J. Thorac. Cardiovasc. Surg.* **2003**, *125*, 481–490. DOI:10.1067/mtc.2003.28

41. Ramanathan T, Shirota K, Morita S, Nishimura T, Huang Y, Zheng X, et al. Left ventricular oxygen utilization efficiency is impaired in chronic streptozotocin-diabetic sheep. *Cardiovasc. Res.* **2002**, *55*, 749–756. DOI:10.1016/s0008-6363(02)00497-2
42. Cardozo RH, de Vroomen M, van Bel F, Baan J, Steendijk P. Simultaneous measurement of right and left ventricular volume by the conductance catheter technique in the newborn lamb. *Neth. Heart J.* **2003**, *11*, 203–209.
43. Hon JK, Steendijk P, Khan H, Wong K, Yacoub M. Acute effects of pulmonary artery banding in sheep on right ventricle pressure-volume relations: Relevance to the arterial switch operation. *Acta Physiol. Scand.* **2001**, *172*, 97–106. DOI:10.1046/j.1365-201X.2001.00844.x
44. Lewinsky RM, Szwarc RS, Benson LN, Ritchie JW. The effects of hypoxic acidemia on left ventricular end-systolic elastance in fetal sheep. *Pediatr. Res.* **1993**, *34*, 38–43. DOI:10.1203/00006450-199307000-00010
45. Gupta KB, Bavaria JE, Ratcliffe MB, Edmunds LH, Jr., Bogen DK. Measurement of end-systolic pressure-volume relations by intra-aortic balloon occlusion. *Circulation* **1989**, *80*, 1016–1028. DOI:10.1161/01.cir.80.4.1016
46. Ahmadian M, Williams AM, Mannozzi J, Konecny F, Hoiland RL, Wainman L, et al. A cross-species validation of single-beat metrics of cardiac contractility. *J. Physiol.* **2022**, *600*, 4779–4806. DOI:10.1113/JP283319
47. Gruslova AB, Cabe AG, Kottam A, Walmsley J, Porterfield JE, Sako EY, et al. Smart Drain for Post-Cardiac Surgery Left Ventricular Volumes Evaluated in Large Animal Models. *Ann. Thorac. Surg.* **2022**, *114*, 2270–2279. DOI:10.1016/j.athoracsur.2021.10.044
48. Mathieu M, El Oumeiri B, Touihri K, Hadad I, Mahmoudabady M, Thoma P, et al. Ventricular-arterial uncoupling in heart failure with preserved ejection fraction after myocardial infarction in dogs—Invasive versus echocardiographic evaluation. *BMC Cardiovasc. Disord.* **2010**, *10*, 32. DOI:10.1186/1471-2261-10-32
49. Iwade M, Nomura M, Uezono S, Ashikari E, Ozaki M. Effects of dopamine and olprinone on ventricular energetics in sevoflurane-induced acute left ventricular depression in dogs. *J. Cardiothorac. Vasc. Anesth.* **2006**, *20*, 358–363. DOI:10.1053/j.jvca.2005.05.021
50. Sun Y, Belenkie I, Wang JJ, Tyberg JV. Assessment of right ventricular diastolic suction in dogs with the use of wave intensity analysis. *Am. J. Physiol. Heart Circ. Physiol.* **2006**, *291*, H3114–H3121. DOI:10.1152/ajpheart.00853.2005
51. Munagala VK, Hart CY, Burnett JC, Jr., Meyer DM, Redfield MM. Ventricular structure and function in aged dogs with renal hypertension: A model of experimental diastolic heart failure. *Circulation* **2005**, *111*, 1128–1135. DOI:10.1161/01.CIR.0000157183.21404.63
52. Karunanithi MK, Feneley MP. Single-beat determination of preload recruitable stroke work relationship: Derivation and evaluation in conscious dogs. *J. Am. Coll. Cardiol.* **2000**, *35*, 502–513. DOI:10.1016/s0735-1097(99)00566-5
53. Leather HA, Segers P, Sun YY, De Ruyter HA, Vandermeersch E, Wouters PF. The limitations of preload-adjusted maximal power as an index of right ventricular contractility. *Anesth. Analg.* **2002**, *95*, 798–804. DOI:10.1097/00000539-200210000-00003
54. Denault AY, Gorcsan J, III, Pinsky MR. Dynamic effects of positive-pressure ventilation on canine left ventricular pressure-volume relations. *J. Appl. Physiol.* **2001**, *91*, 298–308. DOI:10.1152/jappl.2001.91.1.298
55. Atkins BZ, Silvestry SC, Davis JW, Kisslo JA, Glower DD, Jr. Means for load variation during echocardiographic assessment of the Frank-Starling relationship. *J. Am. Soc. Echocardiogr.* **1999**, *12*, 792–800. DOI:10.1016/s0894-7317(99)70183-5
56. Hettrick DA, Pagel PS, Warltier DC. Desflurane, sevoflurane, and isoflurane impair canine left ventricular-arterial coupling and mechanical efficiency. *Anesthesiology* **1996**, *85*, 403–413. DOI:10.1097/00000542-199608000-00023
57. Regan CP, Stump GL, Detwiler TJ, Chen L, Regan HK, Gilberto DB, et al. Characterization of an investigative safety pharmacology model to assess comprehensive cardiac function and structure in chronically instrumented conscious beagle dogs. *J. Pharmacol. Toxicol. Methods* **2016**, *81*, 107–114. DOI:10.1016/j.vascn.2016.05.002
58. McKay RG, Miller MJ, Ferguson JJ, Momomura S, Sahagian P, Grossman W, et al. Assessment of left ventricular end-systolic pressure-volume relations with an impedance catheter and transient inferior vena cava occlusion: use of this system in the evaluation of the cardiotonic effects of dobutamine, milrinone, Posicor and epinephrine. *J. Am. Coll. Cardiol.* **1986**, *8*, 1152–1160. DOI:10.1016/s0735-1097(86)80395-3
59. Kass DA, Yamazaki T, Burkhoff D, Maughan WL, Sagawa K. Determination of left ventricular end-systolic pressure-volume relationships by the conductance (volume) catheter technique. *Circulation* **1986**, *73*, 586–595. DOI:10.1161/01.cir.73.3.586
60. Pilz PM, Ward JE, Chang WT, Kiss A, Bateh E, Jha A, et al. Large and Small Animal Models of Heart Failure with Reduced Ejection Fraction. *Circ. Res.* **2022**, *130*, 1888–1905. DOI:10.1161/CIRCRESAHA.122.320246

61. Charles CJ, Rademaker MT, Scott NJA, Richards AM. Large Animal Models of Heart Failure: Reduced *vs*. Preserved Ejection Fraction. *Animals* **2020**, *10*, 1906. DOI:10.3390/ani10101906
62. Kapur NK, Reyelt L, Crowley P, Richey L, McCarthy J, Annamalai S, et al. Intermittent Occlusion of the Superior Vena Cava Reduces Cardiac Filling Pressures in Preclinical Models of Heart Failure. *J. Cardiovasc. Transl. Res.* **2020**, *13*, 151–157. DOI:10.1007/s12265-019-09916-y
63. Lohmeier TE, Iliescu R. Chronic lowering of blood pressure by carotid baroreflex activation: mechanisms and potential for hypertension therapy. *Hypertension* **2011**, *57*, 880–886. DOI:10.1161/HYPERTENSIONAHA.108.119859